Solar Energy Materials & Solar Cells 95 (2011) S83–S88

Contents lists available at ScienceDirect

Solar Energy Materials & Solar Cells

journal homepage: www.elsevier.com/locate/solmat

Assessment of absorber composition and nanocrystalline phases in $CuInS_2$ based photovoltaic technologies by ex-situ/in-situ resonant Raman scattering measurements

V. Izquierdo-Roca [a], A. Shavel [a], E. Saucedo [b], S. Jaime-Ferrer [c], J. Álvarez-García [d], A. Cabot [a,b], A. Pérez-Rodríguez [a,b,*], V. Bermudez [c], J.R. Morante [a,b]

[a] IN2UB/Departament d'Electrònica, Universitat de Barcelona, C. Martí i Franquès 1, 08028 Barcelona, Spain
[b] IREC, Catalonia Institute for Energy Research, C. Jardins de les Dones de Negre 1, 08930 Sant Adrià del Besòs, Barcelona, Spain
[c] NEXCIS, Zone Industrielle 190 Av. Celestin Coq, 13790 Rousset Cedex, France
[d] Centre de Recerca i Investigació de Catalunya (CRIC), Trav. de Gràcia 108, 08012 Barcelona, Spain

ARTICLE INFO

Article history:
Received 11 August 2010
Received in revised form
28 October 2010
Accepted 21 November 2010
Available online 13 December 2010

Keywords:
$CuIn(S,Se)_2$
Raman scattering
Thin film chalcopyrite technologies

ABSTRACT

This work describes the use of quasi-resonant Raman scattering measurements for the assessment of chemical composition and nanocrystalline phases in $CuInS_2$ based photovoltaic technologies. Raman spectra measured in S-rich $CuIn(S,Se)_2$ layers at a fixed wavelength of 785 nm show a strong increase in the intensity of the peaks that are related to the quasi-resonant excitation of the corresponding vibrational modes. The spectra measured at these conditions are characterised by the presence of seven bands that have been identified with four first order peaks in the 200–400 cm^{-1} spectral region and three second order peaks in the 550–750 cm^{-1} spectral region. These spectra are strongly sensitive to changes in the composition of S-rich $CuIn(Se,S)_2$ alloys. On the other hand, the strong increase in the intensity of the peaks allows the development of in-situ measurements for real time process monitoring. As an example of this application, Raman spectra have been measured at real time conditions during the growth of colloidal $CuInS_2$ nanocrystals that are being developed for the fabrication of low cost solar cells. The data obtained corroborate the potential of quasi-resonant Raman scattering measurements for the development of ex-situ and in-situ quality control and process monitoring tools in thin film chalcopyrite photovoltaic technologies.

1. Introduction

Chalcopyrite based laboratory cells have recently achieved a record efficiency higher than 20% [1]. However, attaining such high efficiency values in commercial modules is challenging due to the narrow process window existing in several steps of the production process. In particular, the performance of photovoltaic (PV) devices is highly sensitive to local changes in the absorber composition, which result in fluctuations of the optoelectronic properties in the absorber layer. This is specially relevant in cells based on quaternary alloys from the $Cu(In,Ga)(S,Se)_2$ system. Changes in the composition of the alloy allow the synthesis of layers within a wide range of bandgap values, from 1.04 eV (corresponding to pure $CuInSe_2$) up to 2.4 eV (corresponding to pure $CuGaS_2$) [2,3]. Due to the strong dependence of the bandgap on the material composition, an accurate control of the alloy composition is required in order to ensure an optimum value of the absorber bandgap. In terms of the production of large area modules, this can be even more critical because variations localized in small areas may result in the degradation of the overall performance of the device.

Improvement in the control of processing conditions requires the development of non-destructive optical monitoring and quality assessment techniques. Raman scattering is specially suited for these applications, due to its ability to provide information on the chemical and microstructural properties of the films, including the quantitative analysis of the chemical composition in quaternary alloys and the identification of secondary phases [4]. The technique is also very well adapted for the analysis of the homogeneity of the layers, as it is possible to achieve diffraction limited spatial resolution ($\sim$1 μm). In addition, the non-destructive optical character of the technique, together with the fact that no sample preparation is required for the analysis, open interesting perspectives for its implementation for in-line and on-line quality control and process monitoring [5]. In this sense, Raman scattering has already been applied to the in-situ characterisation of the growth of $CuInS_2$ layers by sputtering deposition of metallic precursors followed by a sulphurisation step [6]. However, the fast kinetics of many absorber synthesis processes and

* Corresponding author at: IREC, Catalonia Institute for Energy Research, C. Jardins de les Dones de Negre 1, 08930 Sant Adrià del Besòs, Barcelona, Spain.
E-mail addresses: aperezr@irec.cat (A. Cabot), aperezr@irec.cat (A. Pérez-Rodríguez).

0927-0248/$ - see front matter © 2010 Elsevier B.V. All rights reserved.
doi:10.1016/j.solmat.2010.11.014

the low Raman scattering cross section of chalcopyrite materials compromise the applicability of the technique to monitor fast structural and chemical changes. Furthermore, the weak Raman signal also limits the throughput of the technique in applications involving the inspection of absorber modules at an industrial scale.

In this framework, this work describes the use of quasi-resonant Raman scattering measurements for the assessment of chemical composition and nanocrystalline phases in $CuInS_2$ based photovoltaic technologies. Quasi-resonant excitation conditions can be achieved by selecting an excitation wavelength close enough to the bandgap of the alloy [7,8]. This leads to a strong increase in the intensity of the Raman modes, which allows to significantly decrease the integration time. This approach has been applied to the analysis of electrodeposited S-rich $CuIn(S,Se)_2$ absorbers. Single step electrodeposition of a $CuInSe_2$ precursor followed by a reactive annealing under sulphurising conditions constitute an interesting technological approach with significant potential for cost reduction in front of conventional vacuum-based deposition technologies [9,10]. Currently, solar cell efficiencies up to 11% have been demonstrated with these processes. A critical feature in the further optimisation of these technologies is the improvement in the control of the sulphurisation step, which gives a strong interest to the non-destructive assessment of this process.

The analysis of the Raman spectra measured at quasi-resonant conditions in layers synthesised with different [S]/([S]+[Se]) relative contents (from 70% up to 100%) has revealed the very high sensitivity of the measurements to small changes in the alloy composition. This technique constitutes a fast and sensitive tool for the non-destructive assessment of the alloy composition. Moreover, the strong increase achieved in the intensity of the modes when working at quasi-resonant conditions has allowed the development of in-situ measurements for real time process monitoring. As an example of this application, Raman spectra have been measured at real time conditions during the growth of colloidal $CuInS_2$ nanocrystals that are being developed for the fabrication of low cost solar cells [11], reporting the first (to our knowledge) Raman spectra obtained in-situ during the synthesis process of these nanocrystalline phases.

2. Materials and methods

S-rich $CuIn(S,Se)_2$ alloys with different [S]/([S]+[Se]) relative contents (from 70% up to 100%) were synthesised following a two step process: $CuInSe_2$ precursors were grown onto Mo coated glass substrates with a single electrodeposition step in an acidic bath, according to the process described in [12]. The electrochemical bath was prepared using $CuSO_4$ (1×10^{-3} M), SeO_2 (1.7×10^{-3} M), $In_2(SO_4)_3$ (6.0×10^{-3} M) and a supporting sulphate electrolyte, with a pH close to 2, and the electrodeposition conditions were chosen in order to produce precursor layers with a Cu/In content ratio of 1.3. In a second stage, precursors were annealed and subsequently sulphurised in a rapid thermal process (RTP) furnace at 650 °C, obtaining absorber layers with a Cu/In content ratio slightly below 1. Cu/In content ratio in the precursor and absorber layers was measured immediately after their growth by X-ray fluorescence using a Fisherscope X-ray XVD-SD equipment.

$CuInS_2$ nanocrystals were obtained by reacting CuCl and $InCl_3$ with thiourea in a 1,2-dichlorobenzene solution (DCB, 99%, anhydrous) containing dodecanethiol (DDT, 98%) and oleylamine (Tech., 70%). In a typical $CuInS_2$ preparation, CuCl (25 mg; 0.25 mmol), $InCl_3$ (55 mg; 0.25 mmol), 1 g of DDT, 1 g of Oleylamine and 10 g of DCB were placed in a four neck flask and heated up to 150 °C under an argon flow until a yellow transparent solution was formed. The reaction mixture was kept at that temperature for one additional hour for purification. Then the solution was heated to 180 °C and 1 mmol thiourea in 0.5 ml of dimethyl formamide was swiftly injected through a septum. The reaction mixture was kept at 180 °C during additional 40 min to allow the growth of nanoparticles. Finally the solution was rapidly cooled to room temperature.

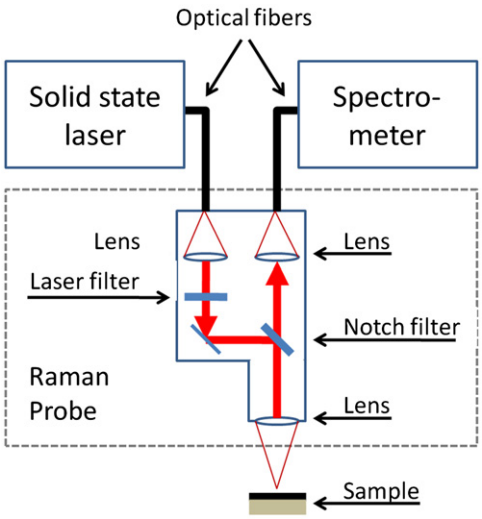

Fig. 1. Schematic representation of the quasi-resonant Raman scattering experimental setup.

Quasi-resonant Raman spectra were measured at the backscattering configuration using a modular BWTEK fibre coupled system suitable for its implementation in different process environments. The system includes a single grating spectrometer (BTC-161-E) coupled to a temperature stabilized solid state laser (wavelength 785 nm) and a Raman probe. The probe contains a band-pass filter to reject the Raman signal from the fibre, as well as a notch filter to minimize stray light in the spectrometer. Fig. 1 is a schematic representation of the Raman scattering experimental setup. For the used excitation wavelength, the penetration depth of scattered light in $CuInS_2$ is estimated to be around 700 nm. The focused spot size on the measured surface was about 100 μm, with an excitation power of 50 mW.

Complementary high resolution Raman measurements (at non-resonant conditions) were made using a T64000 Horiba Jobin–Yvon spectrometer. In this case, excitation was provided with the 514.5 nm emission line of an Ar^+ laser and measurements were also performed in backscattering configuration. For this excitation wavelength, the penetration depth of scattered light in $CuInS_2$ is estimated to be around 100 nm. The focused spot size on the measured surface was about 100 μm, with an excitation power of 20 mW. The chemical composition of the alloys has been estimated by X-ray diffraction (XRD) measurements that were performed in the samples using a Siemens D500 diffractometer. The composition in the $CuIn(S,Se)_2$ alloys was estimated from the shift towards lower angles of the main chalcopyrite peaks in the diffractograms in relation to those corresponding to stoichiometric $CuInS_2$, assuming that the validity of Vegard's law is in agreement with the experimental results reported in [12,13]. Finally, the nanocrystals were characterised by means of Transmission Electron Microscopy (TEM) using a Jeol 1010 microscope operating at 80 kV.

3. Results and discussion

3.1. Analysis of S-rich $CuIn(S,Se)_2$ layers

From the vibrational point of view, the zone centre phonon representation of the chalcopyrite structure is constituted by 21 optical modes, of which only the two A_2 modes are silent [14]: $\Gamma_{opt}=1A_1\oplus2A_2\oplus3\ B_1\oplus3\ B_2\oplus6$ E. Besides, B_2 and E modes present

LO–TO splitting due to their polar character, leading to a relatively complex Raman spectrum. In fact, most of these modes have a very low scattering cross section and overlap each other, and thus are difficult to resolve. Normally, only the A_1 vibrational mode is clearly resolved in the spectra. This can be seen in Fig. 2 (bottom), which shows the Raman spectrum measured on a $CuInS_2$ layer with 514 nm excitation wavelength.

In contrast, the spectrum measured with 785 nm excitation wavelength shows a strong increase in the intensity of the peaks, which is related to the resonant enhancement of the modes. This has allowed to obtain a significant reduction in the integration time, when the integration time used in these measurements was 10 s. Fig. 2 (top) shows the Raman spectrum measured at quasi-resonant conditions, after the subtraction of the luminescence background. This spectrum is characterised by the presence of four first order peaks in the 200–400 cm^{-1} spectral region, and three second order bands in the 550–750 cm^{-1} spectral region. Table 1 lists the frequency of the different peaks from the experimental spectrum, together with the values obtained by Álvarez-García [15] from room temperature measurements and those reported by Koschel and Bettini [14] from polarisation measurements at 78 K. Comparison of these data with those reported in the literature has allowed the assignment of the peaks with different first order vibrational modes and second order peaks characteristic of chalcopyrite ordered $CuInS_2$. In this comparison one has to take into account that increasing the temperature leads to a decrease in the frequency of the modes and, hence, lower frequency values are to be expected from measurements performed at room temperature. For the first order modes, the assignment of the peaks agrees with that previously reported by Wakita et al. [7] from resonant Raman scattering measurements performed at 9 K.

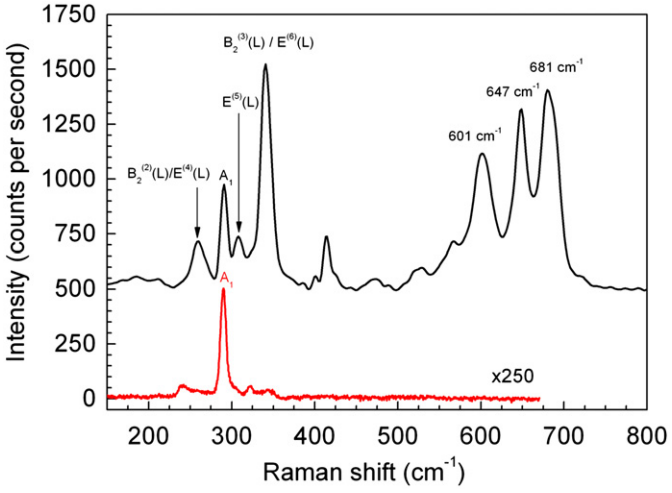

Fig. 2. Raman spectra measured with 785 nm (top) and 514 nm excitation wavelengths (bottom) from a $CuInS_2$ layer, after background subtraction.

Table 1
Frequency of the first and second order Raman modes with their assignment with $CuInS_2$ vibrational modes. The table includes the values obtained for the first order modes by Álvarez-García et al. from measurements performed at room temperature [15] and by Koschel et al. from polarisation measurements at 78 K [14].

Raman shift (cm^{-1}) (this work)	Assignment	Álvarez–García	Koschel et al.
258	$B_2^{(2)}(L)/E^{(4)}(L)$	$B_2^{(2)}(L)$: 260 $E^{(4)}(L)$: 260	$B_2^{(2)}(L)$: 266 $E^{(4)}(L)$: 260
290	A_1	A_1: 290	A_1: 294
307	$E^{(5)}(L)$	$E^{(5)}(L)$: 308	$E^{(5)}(L)$: 314
340	$B_2^{(3)}(L)/E^{(6)}(L)$	–	$B_2^{(3)}(L)$: 352 $E^{(6)}(L)$: 339
601	$[B_2^{(2)}(L)/E^{(4)}(L)]+[B_2^{(3)}(L)/E^{(6)}(L)]$		
647	$E^{(5)}(L)+[B_2^{(3)}(L)/E^{(6)}(L)]$		
681	$[B_2^{(3)}(L)/E^{(6)}(L)]+[B_2^{(3)}(L)/E^{(6)}(L)]$		

The spectra measured at these conditions are also characterised by the presence of a broad luminescence background. This can be seen in Fig. 3, wherein the experimental spectra from samples with different S relative content are plotted without background subtraction. XRD measurements performed in these samples have corroborated the presence of a single quaternary $CuIn(S,Se)_2$ phase in the layers. In the spectra from Fig. 3, both first and second order Raman peaks appear superimposed to the background signal. Observation of this broad luminescence band at room temperature has been already reported by Yakushev et al. [16], who identified this band with the A free exciton peak. The inset in the figure shows the plot of the relative S content in the layers versus the energy of the luminescence peak, as deduced from the fitting of the experimental band with a Gaussian curve. These data point out the existence of a linear dependence of the energy of the A free exciton on the alloy composition. This agrees with the existence of a linear dependence of the bandgap of the alloy on the S relative content as has been already reported from both theoretical and experimental data [17,18].

The dependence of the Raman cross section on the excitation energy due to an incoming resonance can be written approximately as [7,19]:

$$\sigma_i \propto 1/[(E_a - \hbar\omega_i)^2 + \Gamma_a^2] \quad (1)$$

where E_a and Γ_a are the energy and damping constant of the resonant intermediate state, respectively, and $\hbar\omega_i$ is the energy of the incident photons. Fig. 4 shows the intensity of the main mode in the resonant spectra at about 340 cm^{-1} (that has been identified with a $B_2^{(3)}(L)/E^{(6)}(L)$ vibrational mode) versus the bandgap energy of the alloys. The solid line in the figure corresponds to the fitting of these data with Eq. (1), assuming that σ_i equals Raman scattering intensity and resonant Raman scattering in the vicinity of the direct bandgap [19]. The excellent agreement of this theoretical curve with the experimental data confirms the existence of a resonant mediated enhancement of the intensity of the mode.

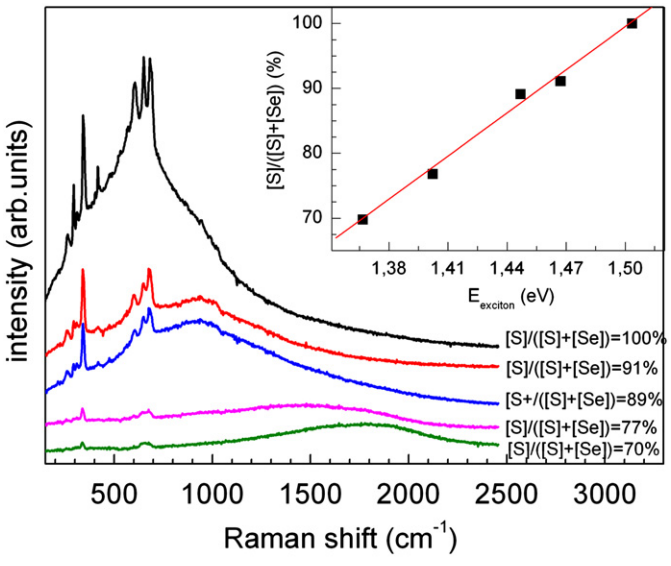

Fig. 3. Experimental Raman spectra measured with 785 nm excitation wavelength on S-rich $CuIn(S,Se)_2$ layers with different composition, without background subtraction. Inset shows the plot of the [S]/([S]+[Se]) relative content versus the photoluminescence exciton energy peak. Full line in the inset is the fitting of the data with a linear relationship.

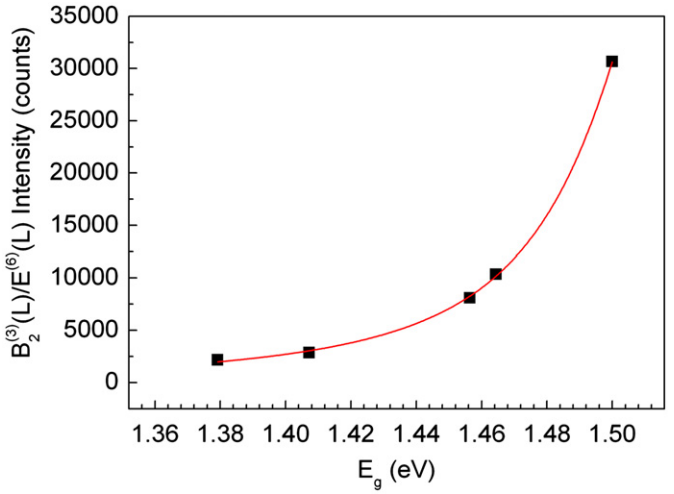

Fig. 4. Intensity of the main mode at 340 cm^{-1} in the spectra measured with 785 nm excitation wavelength versus alloy energy bandgap. Full line corresponds to the fitting of the data with Eq. (1).

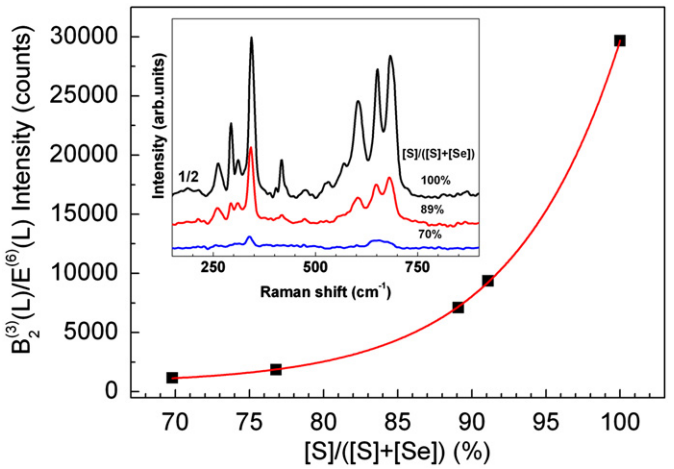

Fig. 5. Dependence of the intensity of the main mode at 340 cm^{-1} in the spectra measured with 785 nm excitation wavelength on the relative S content in the alloy. Full line corresponds to the fitting of the data with the same expression deduced in Fig. 3, taking into account the linear dependence of the bandgap on the alloy composition. Inset shows the evolution of the spectra measured for layers with different composition.

Decreasing the content of S in the alloy leads to a deviation of the bandgap from the quasi-resonant conditions achieved with the 785 nm excitation wavelength, and this determines a strong decrease in the intensity of the peaks in the Raman spectra. This is clearly reflected in Fig. 5, which shows the intensity of the main $B_2^{(3)}(L)/E^{(6)}(L)$ peak in the spectra versus the relative S content in the alloy. The full line in this figure corresponds to the fitting of the data with the same expression deduced in Fig. 4, taking into account the linear dependence of the bandgap on the alloy composition. As shown, changes in the composition of the layer can be easily detected by the corresponding changes in the intensity of the Raman mode, wherein the measurements are especially sensitive to very small changes in the S relative content around the composition corresponding to the highest intensity of the peak. For the experimental conditions used in this work, this corresponds to the $CuInS_2$ ternary compound. By a suitable selection of the excitation wavelength, the measurements can be extended to the analysis of different compositional ranges in quaternary alloys from the $Cu(In,Ga)(S,Se)_2$ system that are currently used for the development of high efficiency devices.

3.2. *In-situ characterisation of the growth of colloidal $CuInS_2$ nanocrystals*

Fig. 6 shows the Raman spectra in-situ measured during the nanoparticles growth with 785 nm (top) and 514 nm (bottom) excitation wavelengths, respectively. The inset of Fig. 6 shows a representative TEM image of the obtained nanoparticles. The $CuInS_2$ nanocrystals finally obtained have average particle sizes in the range 10–15 nm. The spectrum measured under non-resonant excitation conditions shows a peak at about 301 cm^{-1}, in addition to the main $CuInS_2$ A_1 mode at about 290 cm^{-1}. This peak has been identified with the main vibrational mode from the CuAu ordered polytype of $CuInS_2$ [4]. This points out the coexistence in these samples of both chalcopyrite and Cu–Au ordered $CuInS_2$ polytypes. Besides, there is a smaller contribution that appears at about 340 cm^{-1}. The position of this contribution agrees with that of the $B_2^{(3)}(L)/E^{(6)}(L)$ $CuInS_2$ peak in the spectra measured at quasi-resonant conditions. However, the intensity of this band in the spectra measured at non-resonant conditions suggests the band to be related to the presence of a $CuIn_5S_8$ spinel secondary phase [20], wherein the main vibrational peak characteristic from this phase is in the same spectral region as that of the $B_2^{(3)}(L)/E^{(6)}(L)$ $CuInS_2$ mode. This interpretation is supported by the comparison of the relative intensity of this band in relation to the main A_1 mode in the spectra measured at non-resonant conditions with those measured in $CuIn_5S_8$ free films [21]. In addition, the spectrum measured under non-resonant conditions in Fig. 6 also shows a small peak at 470 cm^{-1} that has been identified with the main mode from Cu_xS binary compounds [22]. Presence of these secondary phases has also been assessed by XRD.

Laser excitation with the 785 nm wavelength leads to a strong increase in the intensity of the $CuInS_2$ peak, because of the occurrence of quasi-resonant excitation conditions. This also includes the main vibrational mode from the Cu–Au ordered polytype. The high sensitivity of the spectra due to the presence of these phases and the possibility to perform the measurements with short integration times (of the order of seconds) has allowed their implementation at in-situ conditions during the growth stage of the nanocrystals at 180 °C. Fig. 7 shows the sequence of spectra

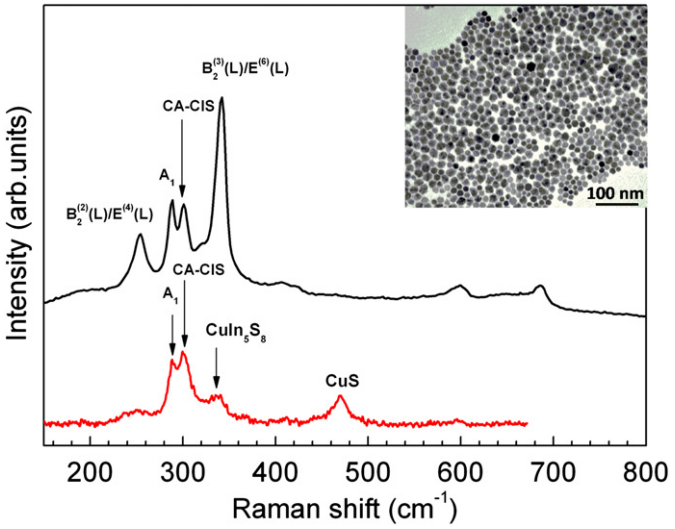

Fig. 6. Raman spectra measured with 785 nm excitation wavelength (top) and 514 nm excitation wavelength (bottom) from the $CuInS_2$ nanoparticles. Inset shows a TEM image of the nanoparticles.

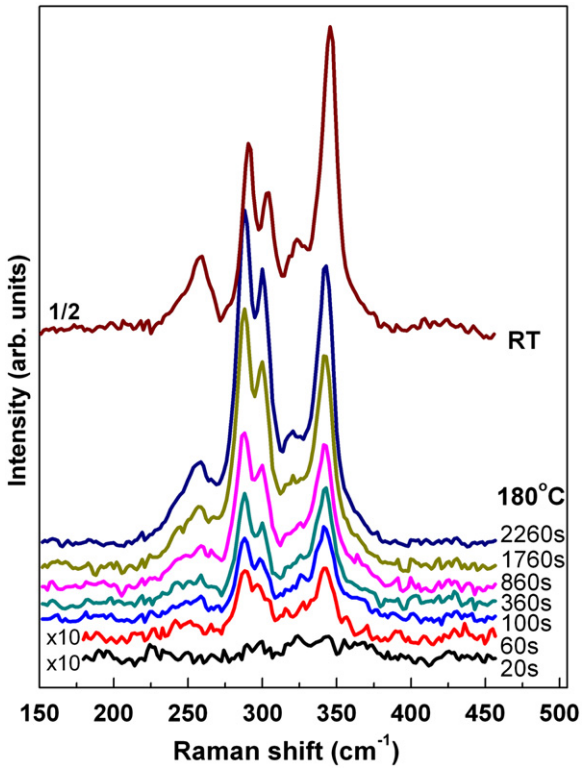

Fig. 7. In-situ Raman monitoring of the nanocrystals growth: Raman spectra measured with 785 nm excitation wavelength during the final process stage at 180 °C.

measured at different crystal growth times. In this figure, it is interesting to remark that all the spectra measured at this temperature with process times longer than 60 s show a similar resonant pattern characterised by the A_1 mode from chalcopyrite $CuInS_2$ as a dominant peak. The relative intensity of the other peaks in the spectra in relation to the main A_1 one is also very similar in all these spectra. These similarities indicate the existence of a similar resonant behaviour of all the corresponding vibrational modes in the different spectra, which suggests similar values of the bandgap of the nanoparticles. It is well known that semiconductor nanocrystals with dimensions lower than the exciton Bohr radius, show a size-dependence of their bandgap energy [23]. Then, the similar resonant pattern in the spectra measured at different times during the process suggests a fast initial nanoparticle growth. After the first 60 s of reaction the particles are already larger than 4.1 nm, which is the exciton Bohr radius for $CuInS_2$ [24]. The further increase in the intensity of the modes with the reaction time is associated to the posterior continuous growth of the particles and the improvement of their crystallographic structure. The changes in the relative intensities of the peaks in the spectrum measured after cooling of the solution down to room temperature are attributed to the differences in the dependence of the intensity of the corresponding modes on temperature.

4. Conclusions

The analysis of quasi-resonant Raman scattering measurements performed at a fixed excitation wavelength of 785 nm on S-rich $CuIn(S,Se)_2$ absorbers has corroborated the potential and capabilities of this kind of measurements for the determination of the relative S content in $CuIn(S,Se)_2$ quaternary alloy layers. Resonant enhancement leads to a strong increase in the intensity of the peaks that show a strong dependence on the relative S content in the layers. Analysis of the broad luminescence background signal in the spectra provides an additional tool for the determination of the layer composition because of the direct linear correlation between the exciton energy and the alloy composition. Resonant Raman Spectroscopy constitutes a fast and non-destructive tool for the detection of deviations in the composition and bandgap of the absorbers. By a suitable selection of the excitation wavelength, the technique can be extended to the investigation of alloys with different compositions within the $Cu(In,Ga)(S,Se)_2$ system. Using microscope optics, mapping measurements with high lateral resolution can be achieved, enabling the analysis of local bandgap and composition inhomogeneities that are strongly relevant for the efficiency of the devices.

In addition, the strong increase achieved in the intensity of the peaks when working at quasi-resonant conditions opens interesting perspectives for the in-situ implementation of the technique for real time process monitoring in processes with high interest for the development of low cost photovoltaic technologies. As an application of this technique, quasi-resonant measurements have been successfully applied for monitoring the colloidal synthesis of $CuInS_2$ nanoparticles. These are the first (to our knowledge) reported data on the in-situ observation of the Raman spectra related to chalcopyrite nanocrystalline phases.

Acknowledgments

Authors from IREC and University of Barcelona belong to the M-2E (Electronic Materials for Energy) Consolidated Research Group and the XaRMAE Network of Excellence on Materials for Energy of the "Generalitat de Catalunya". This work was partly funded by the LARCIS project (Grant no. SES6-CT-2005-019757) from 6th FP of the European Union, and Project ref. FR2009-0014 from the French-Spanish Picasso Cooperative Programme. E. Saucedo also thanks the Spanish Ministry of Science and Innovation for the Juan de la Cierva fellowship.

References

[1] M. Powalla, P. Jackson, E. Lotter, D. Hariskos, S. Paetel, R. Würz, R. Menner, W. Wischmann, New world record efficiency for $Cu(In,Ga)Se_2$ solar cells beyond 20%, presented at the Symposium M, Thin Film Chalcogenide Photovoltaic Materials of the 2010 E-MRS Spring Meeting, Strasbourg, France, June 2010.
[2] F.O. Adurodija, J. Song, I.O. Asia, K.H. Yoon, Formation of $CuIn(S,Se)_2$ thin film by thermal diffusion of sulphur and selenium vapours into Cu-In alloy within a closed graphite container, Sol. Energ. Mater. Sol. C. 58 (1999) 287–297.
[3] E.P. Zaretskaya, V.F. Gremenok, V.B. Zalesski, K. Bente, S. Schorr, S. Zukotynski, Properties of $Cu(In,Ga)(S,Se)_2$ thin films prepared by selenization/sulfurization of metallic alloys, Thin Solid Films 515 (2007) 5848–5851.
[4] R. Scheer, A. Pérez-Rodríguez, W.K. Metzger, Advanced diagnostic and control methods of processes and layers in CIGS solar cells and modules, Prog. Photovolt.: Res. Appl. 18 (2010) 467–480.
[5] V. Izquierdo-Roca, E. Saucedo, J.S. Jaime-Ferrer, X. Fontané, A. Pérez-Rodríguez, V. Bermúdez, J.R. Morante, Raman scattering process monitoring of thin film chalcopyrite technologies: Application for in-situ control of composition of precursors in electrodeposited $CuIn(S,Se)_2$ solar cells, in: Proceedings of the 35th IEEE Photovoltaics Specialists Conference, Hawaii, USA, June 2010.
[6] E. Rudigier, B. Barcones, I. Luck, T. Jawhari-Colin, A. Pérez-Rodríguez, R. Scheer, Quasi real-time Raman studies on the growth of Cu–In–S thin films, J. Appl. Phys. 95 (2004) 5153–5159.
[7] K. Wakita, H. Hirooka, S. Yasuda, F. Fujita, N. Yamamoto, Resonant Raman scattering and luminescence in $CuInS_2$ crystals, J. Appl. Phys. 83 (1998) 443–448.
[8] I.H. Choi, D.H. Lee, Resonance Raman scattering and exciton–phonon interactions in $CuInS_2$, J. Kor. Phys. Soc. 44 (2004) 1542–1546.
[9] J.F. Guillemoles, P. Cowache, S. Massaccesi, L. Thouin, S. Sanchez, D. Lincot, J. Vedel, Solar cells with improved efficiency based on electrodeposited copper indium diselenide thin films, Adv. Mater. 6 (1994) 379–381.
[10] D. Lincot, J.F. Guillemoles, S. Taunier, D. Guimard, J. Sicx-Kurdi, A. Chaumont, O. Roussel, O. Ramdani, C. Hubert, J.P. Fauvarque, N. Bodereau, L. Parissi, P. Panheleux, P. Fanouillere, N. Naghavi, P.P. Grand, M. Benfarah, P. Mogensen, O. Kerrec, Chalcopyrite thin film solar cells by electrodeposition, Sol. Energ. 77 (2004) 725–737.

[11] M.G. Panthani, V. Akhavan, B. Goodfellow, J.P. Schmidtke, L. Dunn, A. Dodabalapur, P.F. Barbara, B.A. Korgel, Synthesis of $CuInS_2$, $CuInSe_2$, and $Cu(In_xGa_{1-x})Se_2$ (CIGS) nanocrystal "Inks" for printable photovoltaics, J. Am. Chem. Soc. 130 (2008) 16770–16777.
[12] S. Taunier, J. Sicx-Kurdi, P.P. Grand, A. Chomont, O. Ramdani, L. Parissi, P. Panheleux, N. Naghavi, C. Hubert, M. Ben-Farah, J.P. Fauvarque, J. Connolly, O. Roussel, P. Mogensen, E. Mahé, J.F. Guillemoles, D. Lincot, O. Kerrec, $Cu(In,Ga)(S,Se)_2$ solar cells and modules by electrodeposition, Thin Solid Films 480–481 (2005) 526–531.
[13] T. Yamaguchi, T. Naoyama, H.S. Lee, A. Yoshida, T. Kobata, S. Niiyama, T. Nakamura, Preparation of $CuIn(S,Se)_2$ thin films by thermal crystallization in sulphur and selenium atmosphere, J. Phys. Chem. Solids 64 (2003) 1831–1834.
[14] W.H. Koschel, M. Bettini, Zone-centered phonons in $A_IB_{III}S_2$ chalcopyrites, Phys. Status Solidi (b) 72 (1975) 729–737.
[15] J. Álvarez-García, Characterisation of $CuInS_2$ films for solar cell applications by Raman spectroscopy, Doctoral Thesis, University of Barcelona, Spain, 2002.
[16] M.V. Yakushev, A.V. Mudryi, Y. Feofanov, A.V. Ivaniukovich, I.V. Victorov, Excitons in high-quality $CuInS_2$ single crystals, Thin Solid Films 511 (2006) 130–134.
[17] M. Turcu, I.M. Kötschau, U. Rau, Band alignments in the $Cu(In,Ga)(S,Se)_2$ alloy system determined from deep-level defect energies, Appl. Phys. A 73 (2001) 769–772.
[18] S. Chavhan, R. Sharma, Growth, structural and optical properties of non-stoichiometric $CuIn(S_{1-x}Se_x)_2$ thin films deposited by solution growth technique for photovoltaic application, J. Phys. Chem. Solids 67 (2006) 767–773.
[19] P.Y. Yu, M. Cardona, Fundamentals of Semiconductors: Physics and Materials Properties, 3rd edition, Springer-Verlag, Berlin Heidelberg New York, 2005.
[20] N.M. Gasanly, S.A. El-Hamid, L.G. Gasanova, A.Z. Magomedov, Vibrational Spectra of Spinel-Type Compound $CuIn_5S_8$, Phys. Status Solidi (b) 169 (1992) k115–K118.
[21] J. Alvarez-García, A. Pérez-Rodríguez, A. Romano-Rodríguez, J.R. Morante, L. Calvo-Barrio, R. Scheer, R. Klenk, Microstructure and secondary phases in coevaporated $CuInS_2$ films: Dependence on growth temperature and chemical composition, J. Vac. Sci. Technol. A 19 (2001) 232–240.
[22] C.G. Munce, G.K. Parker, S.A. Holt, G.A. Hope, A Raman spectroelectrochemical investigation of chemical bath deposited Cu_xS thin films and their modification, Colloids Surfaces A: Physicochem. Eng. Aspects 295 (2007) 152–158.
[23] A.P. Alivisatos, Semiconductor clusters, nanocrystals, and quantum dots, Science 271 (1996) 933–937.
[24] S.L. Castro, S.G. Bailey, R.P. Raffaelle, K.K. Banger, A.F. Hepp, Nanocrystalline chalcopyrite materials ($CuInS_2$ and $CuInSe_2$) via low-temperature pyrolysis of molecular single-source precursors, Chem. Mater. 15 (2003) 3142–3147.